CrystEngComm

Accepted Manuscript

ROYAL SOCIETY OF CHEMISTRY

www.rsc.org/crystengcomm

CrystEngComm

ARTICLE

Optical Properties of Regioregular Poly(3-hexylthiophene) Aggregates From Fully Atomistic Investigations

Received 00th January 20xx,
Accepted 00th January 20xx

DOI: 10.1039/x0xx00000x

www.rsc.org/

Linjun Wang*[,a] and David Beljonne*[,b]

We report on a first-principle theoretical investigation of the optical absorption and emission spectra of poly(3-hexylthiophene) (P3HT) aggregates by means of a multiscale all-atom hybrid approach, which combines: (i) molecular dynamics simulations of (intrachain) conformational and (interchain) positional disorder, (ii) quantum-chemical calculations of intrachain excited states and excitonic interactions, and (iii) solving of a Frenkel-Holstein model that includes coupling of the electronic excitations to a dominant high-frequency molecular vibration. The modeling work points to the co-existence of ordered nano-aggregates into disordered domains, with the former dominating the emission spectrum while both regions contribute to the absorption spectrum. The measured photoluminescence line shape and the Stokes shift are both reproduced by the theory for aggregates comprosing polymer chain with lengths ~35-40 repeating units.

Introduction

Since the first reports on the synthesis of head-to-tail coupled regioregular poly(3-alkylthiophenes) (P3ATs) in the 1990s,[1, 2] poly(3-hexylthiophene) (P3HT) has attracted considerable interest because of its excellent processing properties (e.g. solubility, stability, and flexibility) as well as enhanced electrical conductivity due to the formation of self-organized microcrystalline domains.[3] P3HT has long been considered as a state-of-the-art conjugated polymer for optoelectronic applications, especially in bulk heterojunction (BHJ) organic photovoltaic cells (OPVs) when combined with [6,6]-phenyl-C61-butyric acid methyl ester (PCBM).[4] Among other factors, the optical properties of the P3HT-rich domains are critical in setting up the quantum efficiencies (reported as high as 5.2% in P3HT/PCBM blends[5]) of the OPV devices, as: (1) in PCBM-based solar cells, the amount of sunlight that can be harvested arises primarily from the donor components due to the low absorption cross-section of the fullerene derivatives over the visible-IR regime; and (2) the distance that excitons can travel within their finite lifetime, i.e. the exciton diffusion length, is governed by the spectral overlap between the absorption and emission spectra of the donor molecules in resonant energy transfer processes.[6]

Earlier theoretical investigations of the optical spectra of P3ATs have mostly focused on isolated polymer chains and have revealed the presence of a dominant ring-stretching vibrational mode coupled to the intrachain excitation.[7] In the literature, various models have been proposed to treat the conformational disorder in P3ATs that feature shallow torsional potentials prompting out-of-plane conformations with higher transition energies. At one extreme, strong disorder models consider that the polymer chains break up into a series of electronically non-interacting segments or chromophores that are essentially static over the timescales of the relevant electronic processes.[8] Alternatively, weak disorder models regard the polymer chains as wormlike dynamic objects that explore multiple conformations and thus appear on average essentially planar on short time and length scales.[9, 10] According to these two limiting scenarios that likely prevail in different conditions of temperature, polymer weight distribution, polydispersity and sample preparation, P3HT chains would appear as either multi-chromophoric entities or behave as a single quantum object. For P3HT aggregates, however, interchain interactions can strongly perturb this behavior, either by imposing packing constraints on the backbones and the hexyl side chains (likely freezing out some local polymer conformation degrees of freedom) or by favoring formation of delocalized exciton states. As a result, the optical spectra of realistic P3HT thin films cannot be described by single chains, and thus deserve intensive theoretical investigations.

[a] Department of Chemistry, Zhejiang University, Hangzhou 310027, China.
[b] Laboratory for Chemistry of Novel Materials, University of Mons, Place du Parc 20, B-7000 Mons, Belgium.
*Email: ljwang@zju.edu.cn.; david.beljonne@umons.ac.be

Electronic Supplementary Information (ESI) available: Force field details for P3HT; Experimental and simulated XRD pattern of P3HT crystals; correlation of transition energies in P3HT aggregate (20, 20); chain-length-dependent Huang-Ryns factors, exciton-phonon couplings, transition energies, exciton couplings, absorption peak energies and intensities, and Stokes shifts. See DOI: 10.1039/x0xx00000x

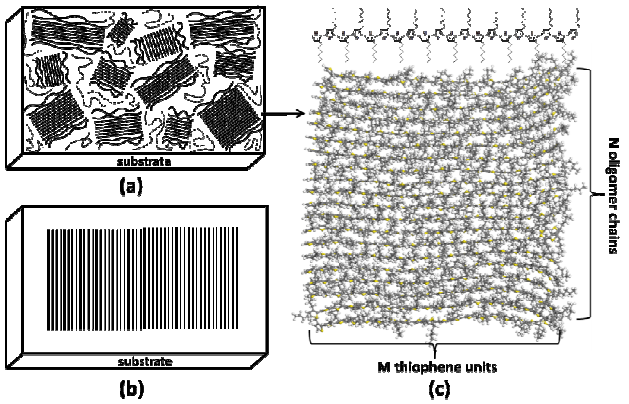

Fig. 1 Schematic presentation of a regioregular P3HT (a) thin film composing of crystalline domains (solid lines) embedded in an amorphous matrix (dashed lines) and (b) nanofiber represented by a stack of ordered long chains. (c) Snapshot of a model P3HT aggregate with N = 20 P3HT oligomer chains and M = 20 thiophene units per chain, together with the chemical structure of a P3HT 20-mer.

P3HT thin films are composed of microcrystalline domains embedded in an amorphous matrix, as illustrated in **Fig. 1a**.[11] Recently, it was found that self-assembly can selectively exclude amorphous regimes and generate P3HT nanofibers of long polymer chains with a distribution of more or less uniform molecular weight (see **Fig. 1b**).[12] From X-ray diffraction (XRD) studies, it was shown that P3HT crystallizes to form lamellae with π-π stacking between the polythiophene backbones and a large segregation induced by the hexyl side chains.[13] P3HT shows multiple polymorphs, e.g., forms I and I' with non-interdigitated hexyl side chains and form II with interdigitation.[14, 15] The unit cell is commonly described as orthorhombic and more detailed investigations show slight deviations pointing at a monoclinic structure.[16]

The optical spectra of P3HT thin films and nanofibers differ significantly. Due to the strong conformational disorder, the chains in the amorphous region have shorter conjugation length and higher excitation energy than the crystalline chains. As a result, all chains contribute to the absorption spectrum of thin films, while only the crystalline chains with low excitation energy determine the emission spectrum. For nanofibers, however, both absorption and emission spectra are expected to stem from the same aggregates. Spano and co-workers have proposed a general phenomenological model to investigate the linear optical response of P3HT aggregates, considering on an equal footing interchain excitonic interactions, exciton-vibration coupling to the dominant ring-stretching mode, and spatially correlated site disorder.[12, 17-21] They pointed out that P3HT aggregates with extremely short and long chains are of H-type and J-type respectively, while the competition between through-bond intrachain coupling and through-space interchain interactions determines the nature of aggregate spectra in intermediate situations. Experimental observations in P3HT thin films and nanofibers[12, 22] have been successfully explained phenomenologically.[23, 24] However, an atomistic description of the optical spectra of P3HT aggregates is still lacking.

In this study, we extend the Spano model to account for all ingredients entering the atomistic description of the primary photoexcitations in P3HT crystalline domains. We aim at revealing the atomistic origin of the absorption and fluorescence emission line shapes and the associated Stokes shift in P3HT aggregates. This is achieved through implementing a hybrid approach combining molecular dynamics simulations to sample (primarily conformational) disorder, quantum-chemical calculations of electronic excitations in individual chains and inter-chain excitonic couplings, and a Frenkel-Holstein model to obtain the optical spectra of P3HT aggregates.

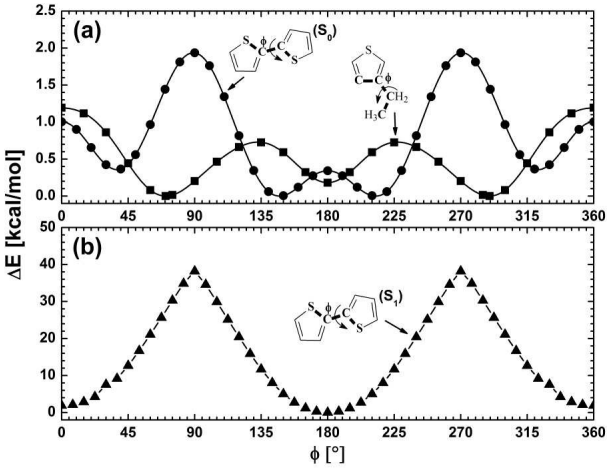

Fig. 2 Calculated torsional potential energy surface of (a) ground state (S_0) 2,2'-bithiophene[25] and 3-ethylthiophene[26] at the MP2/aug-cc-pVTZ level, and (b) first excited state (S_1) 2,2'-bithiophene[26] at the BHHLYP/cc-pVTZ level. The lowest potential in each scan is set to zero.

Methodology

Force-field simulations of polymer conformation and packing

Similar to the work by Moreno et al. dealing with various alkylthiophene-based oligomers and polymers,[27] we adopted the standard parameterization of OPLS-AA force field[28] for the alkyl side chains and reparameterize the potential energy terms related to the thiophene rings. The bond stretching and bond angle bending of the thiophenes were described by the MM3 force field.[29] As shown in **Fig. 2**, the ground (first excited) state torsional potential between the thiophene rings was taken from previous ab initio studies on 2,2'-bithiophene using MP2/aug-cc-pVTZ (BHHLYP/cc-pVTZ).[25, 26] In this study, we also carried out additional *ab initio* calculations with the Gaussian 03 package.[30] The torsional potential between a thiophene ring and an alkane chain was assessed by considering 3-ethylthiophene at the MP2/aug-cc-pVTZ level (see **Fig. 2**). Note that, there exists a sharp transition around 90° on the first excited state potential energy surface (see **Fig. 2b**), indicating that the surface may have crossings with higher excited state surfaces.[31] However, such crossings are inaccessible in our molecular dynamics simulations due to their extremely high energies. Besides, the trimer of thiophene, 2,2':5',2''-terthiophene, was fully optimized at the MP2/cc-pVDZ level, and afterwards a single point calculation was performed at a

higher MP2/aug-cc-pVTZ level. By fitting the *ab initio* molecular electrostatic potential, the atomic point charges of the central thiophene ring were used for the thiophene rings in P3HT.

In order to validate the present force field for the molecular dynamics studies of P3HT, we have next performed XRD pattern simulations[32] for P3HT thin films and compared these to experiment.[13] Based on the experimental crystal structure of poly(3-buthylthiophene),[14] we built up a cubic supercell containing ten P3HT chains, each ten units long, and applied periodic boundary condition in all directions. Different title angles of the thiophene plain with respect to the stack direction were adopted as the starting configurations, and full cell optimization was performed in each case. Both the atomic coordinates and the lattice parameters were optimized through the XTALMIN program implemented in the TINKER 5.1 molecular modeling package.[33] For the most stable optimized molecular packing, the powder diffraction pattern was predicted using the Reflex module in the Material Studio package. In order to simulate the XRD pattern for a thin film, where different domains may have different orientations both along substrate plane and out of the plane, the obtained crystalline pattern is further broadened.[32] The best simulated XRD pattern is displayed in **Fig. S1** of the Supporting Information (SI) together with the corresponding experimental data obtained by Prosa et al. on solution-cast films.[13] Note that similar packing has also been reported in single crystals of P3HT, but with interdigitated hexyl side groups.[34] The main scattering peaks in the experimental pattern are well reproduced by the calculations. The inter-lamellae spacing, the intra-lamella chain-to-chain stacking distance, and the intrachain repeated distances are calculated to be 16.81 Å, 3.77 Å and 8.13 Å, respectively, agreeing very well with the experimental values of 16.8 Å, 3.8 Å and 7.9 Å.[13] We can thus reasonably conclude that our force field is able to describe the supramolecular organization in the P3HT aggregates encountered in thin films, and can be safely used for further molecular dynamics studies on P3HT aggregates.

Quantum-chemical calculations and model Hamiltonian

The P3HT aggregates under investigation are molecular stacks containing N P3HT chains with M thiophene rings per chain, which are denoted as (N, M) hereafter. With the consideration of the computational cost, we choose two series of P3HT model aggregates. Aggregates {(N, 20), N = 5, 10, 15, and 20} are used to investigate the role of aggregate size, while aggregates {(10, M), M = 10, 15, 20, 25, 30, 35, and 40} allow assessing the role of conjugation length. In **Fig. 1c**, we show an example of such an aggregate, i.e., a 20-chain stack of P3HT 20-mer. Each aggregate is embedded in a unit cell with lattice constants at least 50 Å larger than the crystalline phase in order to avoid the interaction of a molecule with its image when applying periodic boundary conditions. Molecular dynamics were performed in the NVT ensemble at 300K. The RATTLE algorithm[35] within TINKER was used to constrain all the bond lengths to be fixed at their equilibrium lengths, and thus the effect of the corresponding high frequency modes was neglected in the classical molecular dynamics (and re-introduced at the quantum-mechanical level). The simulation time was set to be 350 ps with a time interval of 1 fs and the dynamic trajectory were extracted every 50 fs after thermal equilibration of 100 ps with a total number of 5000 snapshots.

The atomic coordinates of each P3HT chain in the aggregate were extracted along the MD run and used as input for intramolecular excited-state calculations at the single configuration interaction (SCI) level. Here, we used the semi-empirical intermediate neglect of differential overlap (INDO) method as parameterized by Zerner for spectroscopic applications,[36] which has been proved to be a good compromise between accuracy and computational cost even for very long oligomers.[37] The exciton couplings between neighboring chains in the aggregate were calculated based on the INDO/SCI transition densities, thus going beyond the simple point dipole interaction model.[38] We are only interested in the low-energy part of the optical absorption spectra, and thus we assume that each P3HT chain in the aggregate has only two electronic states, i.e. the ground state (S_0) and the first excited state (S_1), which are coupled to an intramolecular symmetric vinyl-stretching mode at ~1400 cm^{-1}.[19, 20] Since these vibrations are of high frequency, it is widely assumed that their curvatures are identical but the potential surface is displaced with respect to each other. The one-exciton Hamiltonian to characterize the aggregate reads:

$$H = \sum_n (\omega_{0-0}^n + D)|n\rangle\langle n| + \sum_{mn} J_{mn}|m\rangle\langle n| + \omega_0 \sum_n b_n^\dagger b_n + \omega_0 \lambda \sum_n (b_n^\dagger + b_n)|n\rangle\langle n| + \lambda^2 \omega_0 \quad (1)$$

Here, ω_{0-0}^n is the gas phase $S_0 \rightarrow S_1$ transition energy, D is the gas-to-aggregate transition energy shift due to nonresonant second-order dispersion forces, J_{mn} is the exciton coupling between chain m and n, $|n\rangle$ is a pure electronic state of the aggregate with chain n excited to S_1 while all others remain in their ground-state S_0, $b_n^\dagger$ (b_n) is the creation (annihilation) operator for the S_0 vibrational quanta on chain n, $\lambda = S^{1/2}$ is the exciton-phonon coupling constant related to the Huang-Rhys factor S, which is here calculated at the semi-empirical AM1/SCI level on the basis of the optimized ground- and excited-state geometries (a 2M active space for both occupied and unoccupied molecular orbitals was used to ensure size consistency). Note that zero point energy corresponds to the energy of the state with no electronic or vibrational excitations. The two-particle approximation (TPA), which was firstly introduced by Philpott,[39] can dramatically reduce the basis set size with only a slight sacrifice in accuracy.[40] Using TPA as well as the time-dependent exciton parameters calculated at the atomistic level (namely excitation energies of single polymer chains and excitonic couplings among them), the Hamiltonian matrix, Eq. (1), is constructed and diagonalized to obtain the eigenstates, $|\Psi^{(j)}\rangle$, and associated eigenenergies, $\varepsilon^{(j)}$. The dimensionless polarized absorption spectrum along direction δ is then calculated as:[41]

$$A_\delta(\omega) = (NW_a(0)\mu^2)^{-1} \sum_j \left|\langle G|\mathbf{M}_\delta|\Psi^{(j)}\rangle\right|^2 W_a(\omega - \varepsilon^{(j)}) \cdot \quad (2)$$

Here, **M** is the transition dipole moment operator of the aggregate, which allows one-photon excitation from the aggregate ground state, $|G\rangle$, to the j-th eigenstate, $|\Psi^{(j)}\rangle$, $W_a(\omega)$ is the line shape function representing homogeneous broadening. The emission spectrum along direction δ takes the form:[41]

$$S_\delta(\omega) = (W_e(0))^{-1} \sum_{v_t, t=0,1,2,\ldots} I_\delta(v_t)(1 - v_t\omega_0 / \omega_{em})^3 W_e(\omega - \omega_{em} + v_t\omega_0) \cdot \quad (3)$$

Here, ω_{em} is the frequency of the emitting state, $W_e(\omega)$ is the emission line shape function which is taken as a Gaussian broadening in this study, and $I_\delta(v_t)$ is the dimensionless 0-v_t line strength for the δ-polarized emission, which is given by:

$$I_\delta(v_t) = \mu^{-2} \sum_{\{v_n\}}{}' \left| \left\langle \Psi^{(em)} \middle| \hat{M}_\delta \prod_n |g_n, v_n\rangle \right| \right|^2 \cdot \quad (4)$$

Here, $\prod_n|g_n,v_n\rangle$ is a terminal state in the emission event in which the chain at n is in the electronic ground state with v_n vibrational quanta in the ground state potential. The prime on the summation in Eq. (4) indicates the constraint $\sum_n v_n = v_t$. In this study, we report ensemble averaged properties. Namely, the obtain spectra are averaged over the inhomogeneous disorder sampled along the MD runs, and the homogeneous disorder is taken into account as a broadening to the calculated spectra (Eqs. 2 and 3). The gas-to-aggregate transition energy shift and the homogeneous broadenings are adjusted to reproduce the experimental spectra, while all other parameters are calculated numerically.

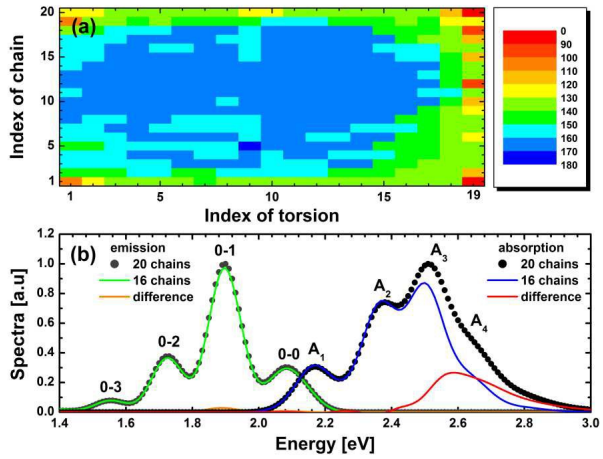

Fig. 3 (a) Distribution of the mean absolute values for all the inter-thiophene-ring torsions and (b) simulated absorption and emission spectra at 300 K of a P3HT aggregate (20, 20). The spectrum based when retaining only the central 16 chains is also shown, together with its difference with respect to the spectrum for the full (20 chains) aggregate. The force field based on the ground state inter-thiophene-ring potential energy surface is used in the molecular dynamics, and a broadening of 0.04 eV is adopted to simulate the spectra.

Results and discussion

Aggregate (20,20) as a reference

The optical spectra of P3HT aggregates strongly depend on the degree of conformational disorder, which is mostly contributed by the inter-thiophene-ring torsions. In **Fig. 3a**, we show the distribution of the mean absolute values for all the inter-thiophene torsions in a typical P3HT aggregate (20, 20). While the very central P3HT chains are quite planar, the backbones get more and more distorted as we move from the inner to the outer chains. Especially, the terminal two chains at the top and the bottom sides of the aggregate show much larger flexibility in comparison with all other 16 internal chains. This is mainly due to the fact that there are more degrees of freedom for these terminal chains, and thus less resistance for thiophene ring rotation. To reduce finite size effects, we thus take the central 16 chains out and calculate their absorption and emission spectra (see **Fig. 3b**). The difference between the spectra using the whole aggregate of 20 chains and that with only the central 16 chains is also shown as a fingerprint for the contribution from the disordered part of the aggregate. From **Fig.3**, it is clearly seen that the central 16-chain aggregate almost exactly reproduce all the features of the measured emission spectrum, and we thus conclude that the emission spectrum is dominated by the more ordered central part. However, the absorption spectrum has important contributions from both the ordered and disordered parts: the former is responsible for the lower energy peaks, i.e., A_1 and A_2, while the latter contributes mostly to the higher and broader energy bands, e.g., A_3 and A_4. Kasha's empirical rule states that photon emission occurs from the lowest excited state,[42] hence from the ordered part of the aggregate. Our modeling work is thus consistent with a picture where the P3HT aggregates are formed by an ordered inner region surrounded by (conformationally) disordered outer chains. Since we are mostly interested in the luminescence and low-energy part of the absorption spectra, we focus below on the central part of the aggregates, removing the two most external polymer chains. Note that recent studies indicate that Kasha's rule may be violated when the first excited state is dark and the transition from the second excited state to the ground state is responsible for fluorescence.[43]

Due to the van der Waals and Coulombic interaction between neighboring chains, the excitation energies of individual chains are generally correlated. In the work by Spano and co-workers, the correlation between the excitation energies of chain m and n, $corr(m,n)$, is normally assumed to decay exponentially with the distance, $|m\text{-}n|$, namely, $corr(m,n)=exp(-|m\text{-}n|/l_0)$, were l_0 is the spatial correlation length.[17-21] **Fig. S2a** shows the correlation function $corr(m,n)$ as calculated in the central part (16 inner chains) of a (20, 20) P3HT aggregate. Our calculations are also consistent with some degree of spatial correlation at least within the central part of the aggregate. There, an exponential fit, shown in **Fig. S2b**, yields a spatial correlation length of l_0 = 2.2. We note that l_0 was set to be 3.5 to best reproduce the experimental temperature dependence of emission spectra in model studies.[21] The predicted value from our atomistic calculations is slightly smaller, likely because the investigated aggregates are placed in vacuum and the environmental contribution to the interchain correlation is missing.

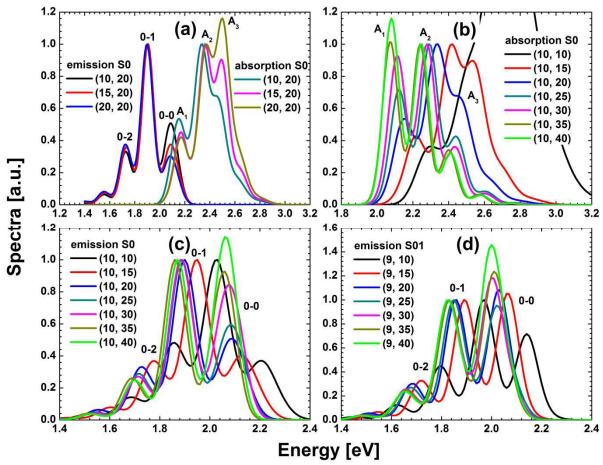

Fig. 4 Simulated (a) absorption and emission spectra of P3HT aggregates {(N, 20), N = 10 ~ 20} with S_0 force field, (b) absorption and (c) emission spectra of aggregates {(10, M), M = 10 ~ 40} with S_0 force field, and (d) emission spectra of aggregates {(9, M), M = 10 ~ 40} with S_1 force field for the central molecule and S_0 force field for the others. Temperature is 300 K and a broadening of 0.04 eV is used for all calculations. All emission (absorption) spectra are normalized by the corresponding intensity of 0-1 (A_2) peaks.

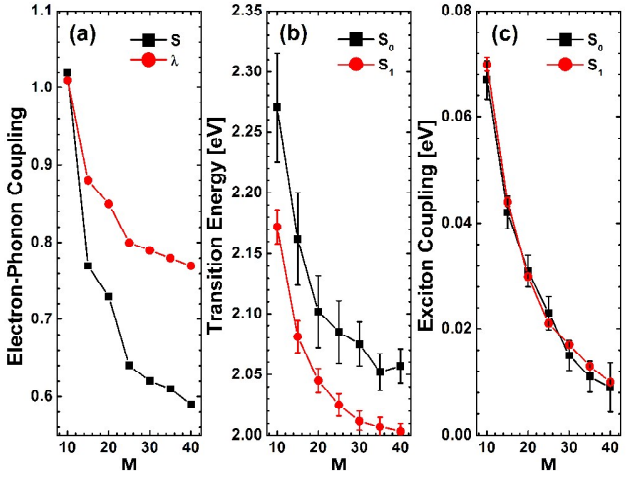

Fig. 5 The chain-length-dependence of (a) Huang-Ryns factor, S, and exciton-phonon coupling constant, λ, (b) first transition energy, and (c) exciton coupling between the nearest chains for P3HT aggregates {(10, M), M = 10, 15, 20, 25, 30, 35, and 40}. The force fields used in the molecular dynamics are based on ground state (S_0) or first excited state (S_1) torsional potentials.

Impact of aggregate size

The role of aggregate size on the optical spectra of P3HT aggregates is shown on **Fig. 4a**. With the increase of the number of chains in the aggregate, the emission spectrum remains more or less the same except for the 0-0 peak, whose intensity is gradually reduced. For disorder-free H-aggregates, we know that the transition dipole moment between the ground state and the lowest excited state is null by symmetry, and thus the 0-0 emission is forbidden. Adding disorder breaks translational symmetry and turns on 0-0 emission. P3HT aggregates formed by short oligomers are H-aggregates, and thus the 0-0 to 0-1 emission intensity ratio is an effective probe for the amount of disorder.[21] The central chains in our P3HT aggregates show increased order in larger aggregates because of reduced edge effects, therefore the relative intensity of the 0-0 emission is lowered. Similar effects are responsible for the reduction of the A_1 intensity in the absorption spectra. Anyway, the line shapes of the absorption and emission spectra vary modestly with the aggregate size and clusters of about 10 chains already capture most of the features obtained for the optical spectra of the largest aggregates. In particular, aggregates formed with long polymer chains show relatively low interchain exciton couplings (see also **Fig. 5 and Table S1**), hence convergence with aggregate size is reached faster. In addition, the Stokes shift is almost size-independent. The following calculations refer therefore to aggregates comprising ten individual chains.

Optical lineshapes

We now move to P3HT aggregates with varying chain lengths. For conjugated polymers like P3HT, electron delocalization along the polymer backbones is enhanced in extended chains. As a result, the nuclear reorganization taking place in the excited state is weaker for longer chains and the corresponding Huang-Rhys factor is smaller (**Fig. 5a**). For the same reason, the transition energy also decreases monotonously with increasing chain length (**Fig. 5b**). The disorder in transition energies using the excited-state torsional potential is about two to three times larger than that using the ground-state potential in the molecular dynamics (since the geometry of the first excited state is more rigid than the ground state structure), see **Fig. 2**. The calculated exciton couplings decrease quickly with the chain length because exciton couplings are driven by dipole-dipole interactions (**Fig. 5c**). The limited variance in the predicted exciton couplings validates our choice of using a Holstein Hamiltonian (see Eq. 1) without Peierls nonlocal electron-phonon couplings.

The calculated absorption and emission spectra for P3HT aggregates with different chain lengths and using the ground-state torsional potential are shown in **Fig. 4b** and **Fig. 4c**, respectively. The corresponding peak energies and relative intensity ratios are given in **Table S2**. Both the absorption and the emission peaks red shift with increasing conjugation length, in line with the changes in calculated excitation energies in **Fig. 5b**. With the increase in chain length, the exciton couplings between the nearest chains in P3HT aggregates reduce quickly, and thus the H character is also weakened accordingly. As a result, the absorption is redistributed to the lower energy side, while the emission moves towards the higher energy side. Using the intensities of the 0-1 and A_2 peaks as reference for emission and absorption, respectively, the 0-0 and A_1 intensities monotonously increase with extended conjugation. The intensity ratio between 0-2 and 0-1 emissions reflects the strength of exciton-phonon couplings and the Huang-Rhys

factor, which is smaller for longer chains, thus rationalizing the weaker 0-2 emission. Although the line shapes of the absorption and emission spectra as calculated in long-chain aggregates agree well with the experimental data in P3HT nanofibers,[12] the predicted Stokes shift (0.01 eV and 0.02 eV for 35-mers and 40-mers, respectively) is much smaller than the experimental value of 0.07 eV (see **Table S2**).

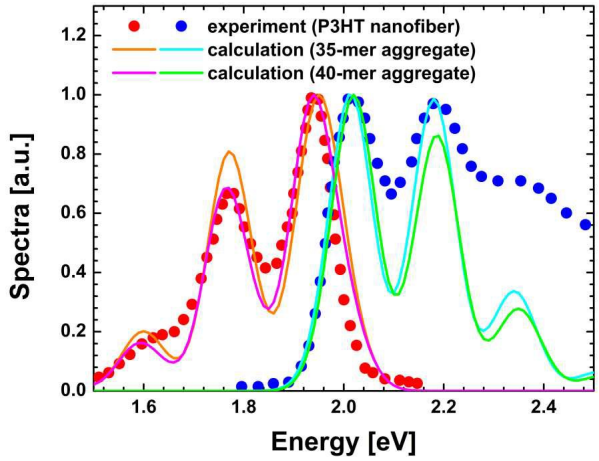

Fig. 6 Room-temperature absorption and emission spectra of calculated P3HT aggregates formed by 35-mers and 40-mers, together with the experimental spectra of P3HT nanofibers.[12] All the calculated spectra are red shifted for 0.06 eV, and a Gaussian broadening of 0.04 eV is used.

Stokes shift

Fig. 2 shows that while the relaxed S_0 geometry adopts a twisted conformation, equilibration in the S_1 excited state favors a planar arrangement. Also, the energy barrier to change from the anti-conformation to the cis-conformation in S_0 is about 2 kcal/mol, which is twenty time less than that in S_1 (about 40 kcal/mol). As a result, P3HT chains tend to relax to a more in-plane conformation after photoexcitation, a geometric relaxation process that is accompanied by a lowering of the transition energies as probed during emission. This effect cannot be properly accounted for when using the ground-state torsional potential in the molecular dynamics simulations. To get around this issue, we applied a hybrid force field, where the torsional potential energy surface of the central chain is switched to the excited-state potential upon excitation, while the other chains retain their the ground-state potentials. This approach is applied to aggregates {(9, M), M = 10 ~ 40} and the corresponding emission spectra reported on **Fig. 4d**. There, the 0-0 emission is enhanced because the electronic excitations involved in emission are spatially confined. Most importantly, the Stokes shift is enlarged because the emission spectrum is red-shifted owing to the smaller transition energy of the more planar emitting conformers. A perfect matching with experimental absorption and emission spectra of P3HT nanofibers is obtained with model aggregates formed by 35-mers and 40-mers, respectively (see **Fig. 6**). Note that a rigid red shift of 0.06 eV is used in all calculated spectra, which accounts for the gas-to-aggregate transition energy shift in the Hamiltonian (Eq. 1).

For P3HT thin films, the Stokes shift of about 0.22 eV is much larger than that of nanofibers (**Table S2**).[19] This cannot be reproduced with the models used here, whatever the physical size of the aggregates and the conjugation length of the polymer chains. We propose two possible scenarios that could potentially explain the large Stokes shift measured in P3HT thin films. The first possibility relies on efficient inter-aggregate energy transfer. There, optical absorption would be dominated by domains constituted of shorter polymer chain lengths with relatively large transition energies, the resulting excitons would then immigrate to and emit from P3HT domains made of longer chain lengths with lower exciton energies. From the data in **Table S2**, the measured Stokes shift would be consistent with absorption and emission from, on average, 15-mers and 40-mers, respectively. The positive exciton couplings and the energetic disorder in P3HT aggregates should also play an important role in modulating the energy of the emitting states. However, their effects cancel out to a large extend (compare Fig. 4c and Fig. 5b), and thus the mean transition energy of the individual polymer chains seems to provide a dominant contribution to the overall Stokes shift. An alternative explanation is that the locally excited electronic states could mix with charge-transfer states. The resulting excimer-like state would then be pushed below the excitonic singlet emission,[44] which would also result in a red shift of the emission spectrum and thus contributes to the Stokes shift.

In principle, coupling between electronic excitations includes two contributions, namely a long-range dipole-dipole Coulombic interaction and a short-range electronic overlap interaction.[45] The former is generally considered to be essential for Förster energy transfer[46] and optical spectra[47, 48] simulations. Recently, Aragó and Troisi found that the latter contribution could also be important for exciton transport along molecular stacks at van der Waals distances.[49] Short-range couplings have also been demonstrated to play an important role in singlet fission dynamics.[50, 51] Yamagata et al. have found the short-range coupling between two P3HT chains to be H-like, which can be added constructively to the usual long-range part.[52] In the present study, we have followed the usual recipe and only took into account the long-range contribution to the excitonic couplings. Inclusion of the short-range part could contribute large fluctuations in the exciton interactions and potentially affect the main characteristics of the absorption and emission spectra. These effects are currently being investigated in our laboratory.

Conclusions

We have systematically investigated the optical absorption and emission spectra for various P3HT model aggregates at the atomistic level. A hybrid approach has been proposed that combines molecular dynamics simulations of the conformational and positional disorder within the aggregate, quantum-chemical calculations of excited states in isolated polymer chains and the use of a Holstein Hamiltonian to account for coupling with intramolecular vibration on an equal footing. We have analyzed the role of aggregate size and

conjugation length on the spectral line shapes and Stokes shift. The picture that emerges from our calculations is consistent with the view that the nanofibers comprise a central ordered domain surrounded by disordered chains, with the former dominating the emission spectrum and the disordered region contributing only to high-energy absorption. Both the optical line shapes and Stokes shift measured on P3HT nanofibers are reproduced for small-size aggregates of relatively long (35-mers or 40-mers) polymer chains, provided planarization of the chains in the excited state is accounted for.

Acknowledgements

We thank Prof. Frank Spano for constructive discussions, Dr. Andrea Minoia for the help in preparing the force field and Dr. Patrick Brocorens for the help of simulating XRD. LW acknowledges support from the "Thousand Young Talents Plan" of China and the "Hundred Talents Plan" of Zhejiang University. The work in Mons was supported by the Interuniversity Attraction Pole program of the Belgian Federal Science Policy Office (PAI 6/27), FNRS-FRFC, and the EC 7th Framework Program under Grant Agreement No. 212311 of the ONE-P project. DB is a FNRS Research Director.

Notes and references

1.R. D. McCullough and R. D. Lowe, *J. Chem. Soc., Chem. Commun.*, 1992, 70-72.
2.T. A. Chen and R. D. Rieke, *J. Am. Chem. Soc.*, 1992, **114**, 10087-10088.
3.H. Sirringhaus, P. J. Brown, R. H. Friend, M. M. Nielsen, K. Bechgaard, B. M. W. Langeveld-Voss, A. J. H. Spiering, R. A. J. Janssen, E. W. Meijer, P. Herwig and D. M. de Leeuw, *Nature*, 1999, **401**, 685-688.
4.R. Kroon, M. Lenes, J. C. Hummelen, P. W. M. Blom and B. de Boer, *Polym. Rev.*, 2008, **48**, 531-582.
5.M. D. Irwin, D. B. Buchholz, A. W. Hains, R. P. H. Chang and T. J. Marks, *Proc. Natl. Acad. Sci. USA*, 2008, **105**, 2783-2787.
6.G. D. Scholes, *Annu. Rev. Phys. Chem.*, 2003, **54**, 57-87.
7.M. Sundberg, O. Inganäs, S. Stafström, G. Gustafsson and B. Sjögren, *Solid State Commun.*, 1989, **71**, 435-439.
8.W. R. Salaneck, O. Inganäs, B. Thémans, J. O. Nilsson, B. Sjögren, J. E. Österholm, J. L. Brédas and S. Svensson, *J. Chem. Phys.*, 1988, **89**, 4613-4619.
9.G. Wenz, M. A. Mueller, M. Schmidt and G. Wegner, *Macromol.*, 1984, **17**, 837-850.
10.Z. G. Soos and K. S. Schweizer, *Chem. Phys. Lett.*, 1987, **139**, 196-200.
11.T.-A. Chen, X. Wu and R. D. Rieke, *J. Am. Chem. Soc.*, 1995, **117**, 233-244.
12.E. T. Niles, J. D. Roehling, H. Yamagata, A. J. Wise, F. C. Spano, A. J. Moulé and J. K. Grey, *J. Phys. Chem. Lett.*, 2012, **3**, 259-263.
13.T. J. Prosa, M. J. Winokur, J. Moulton, P. Smith and A. J. Heeger, *Macromol.*, 1992, **25**, 4364-4372.
14.P. Arosio, M. Moreno, A. Famulari, G. Raos, M. Catellani and S. V. Meille, *Chem. Mater.*, 2009, **21**, 78-87.
15.T. J. Prosa, M. J. Winokur and R. D. McCullough, *Macromol.*, 1996, **29**, 3654-3656.
16.M. Brinkmann and P. Rannou, *Macromol.*, 2009, **42**, 1125-1130.
17.F. C. Spano, *J. Chem. Phys.*, 2005, **122**, 234701.
18.F. C. Spano, *Chem. Phys.*, 2006, **325**, 22-35.
19.J. Clark, C. Silva, R. H. Friend and F. C. Spano, *Phys. Rev. Lett.*, 2007, **98**, 206406.
20.J. Clark, J.-F. Chang, F. C. Spano, R. H. Friend and C. Silva, *Appl. Phys. Lett.*, 2009, **94**, 163306.
21.F. C. Spano, J. Clark, C. Silva and R. H. Friend, *J. Chem. Phys.*, 2009, **130**, 074904.
22.M. Baghgar, J. Labastide, F. Bokel, I. Dujovne, A. McKenna, A. M. Barnes, E. Pentzer, T. Emrick, R. Hayward and M. D. Barnes, *J. Phys. Chem. Lett.*, 2012, **3**, 1674-1679.
23.H. Yamagata and F. C. Spano, *J. Chem. Phys.*, 2012, **136**, 184901.
24.F. Paquin, H. Yamagata, N. J. Hestand, M. Sakowicz, N. Bérubé, M. Côté, L. X. Reynolds, S. A. Haque, N. Stingelin, F. C. Spano and C. Silva, *Phys. Rev. B*, 2013, **88**, 155202.
25.G. Raos, A. Famulari and V. Marcon, *Chem. Phys. Lett.*, 2003, **379**, 364-372.
26.G. Macchi, B. M. Medina, M. Zambianchi, R. Tubino, J. Cornil, G. Barbarella, J. Gierschner and F. Meinardi, *Phys. Chem. Chem. Phys.*, 2009, **11**, 984-990.
27.M. Moreno, M. Casalegno, G. Raos, S. V. Meille and R. Po, *J. Phys. Chem. B*, 2010, **114**, 1591-1602.
28.W. L. Jorgensen, D. S. Maxwell and J. Tirado-Rives, *J. Am. Chem. Soc.*, 1996, **118**, 11225-11236.
29.N. L. Allinger, Y. H. Yuh and J. H. Lii, *J. Am. Chem. Soc.*, 1989, **111**, 8551-8566.
30.M. J. Frisch et al., Gaussian 03, Gaussian Inc, Wallingford, CT 2004.
31.D. Jose and A. Datta, *Cryst. Growth Des.*, 2011, **11**, 3137-3140.
32.P. Brocorens, A. Van Vooren, M. L. Chabinyc, M. F. Toney, M. Shkunov, M. Heeney, I. McCulloch, J. Cornil and R. Lazzaroni, *Adv. Mater.*, 2009, **21**, 1193-1198.
33.J. W. Ponder, TINKER: Software Tools for Molecular Design, 5.1 ed., Washington University School of Medicine, Saint Louis, MO, 2003.
34.K. Rahimi, I. Botiz, N. Stingelin, N. Kayunkid, M. Sommer, F. P. V. Koch, H. Nguyen, O. Coulembier, P. Dubois, M. Brinkmann and G. Reiter, *Angew. Chem. Int. Ed.*, 2012, **51**, 11131-11135.
35.H. C. Andersen, *J. Comput. Phys.*, 1983, **52**, 24-34.
36.M. C. Zerner, Computational Chemistry, edited by D. B. Boyd (Wiley VCH, New York, 1994), Vol. II, p313.
37.J. Gierschner, J. Cornil and H. J. Egelhaaf, *Adv. Mater.*, 2007, **19**, 173-191.
38.J. Gierschner, Y.-S. Huang, B. Van Averbeke, J. Cornil, R. H. Friend and D. Beljonne, *J. Chem. Phys.*, 2009, **130**, 044105.
39.M. R. Philpott, *J. Chem. Phys.*, 1971, **55**, 2039-2054.
40.F. C. Spano, *J. Chem. Phys.*, 2002, **116**, 5877-5891.
41.H. Sun, Z. Zhao, F. C. Spano, D. Beljonne, J. Cornil, Z. Shuai and J. L. Brédas, *Adv. Mater.*, 2003, **15**, 818-822.
42.M. Kasha, *Discuss. Faraday Soc.*, 1950, **9**, 14-19.

43.S. Basak, N. Nandi, K. Bhattacharyya, A. Datta and A. Banerjee, *Phys. Chem. Chem. Phys.*, 2015, **17**, 30398-30403.
44.H. Yamagata, J. Norton, E. Hontz, Y. Olivier, D. Beljonne, J. L. Brédas, R. J. Silbey and F. C. Spano, *J. Chem. Phys.*, 2011, **134**, 204703.
45.N. J. Hestand and F. C. Spano, *J. Chem. Phys.*, 2015, **143**, 244707.
46.T. Förster, *Ann. Phys. (Berlin)*, 1948, **437**, 55-75.
47.M. Kirkus, L. J. Wang, S. Mothy, D. Beljonne, J. Cornil, R. A. J. Janssen and S. C. J. Meskers, *J. Phys. Chem. A*, 2012, **116**, 7927-7936.
48.S. T. Salammal, J.-Y. Balandier, J.-B. Arlin, Y. Olivier, V. Lemaur, L. J. Wang, D. Beljonne, J. Cornil, A. R. Kennedy, Y. H. Geerts and B. Chattopadhyay, *J. Phys. Chem. C*, 2014, **118**, 657-669.
49.J. Aragó and A. Troisi, *Phys. Rev. Lett.*, 2015, **114**, 026402.
50.L. J. Wang, Y. Olivier, O. V. Prezhdo and D. Beljonne, *J. Phys. Chem. Lett.*, 2014, **5**, 3345-3353.
51.D. Beljonne, H. Yamagata, J. L. Brédas, F. C. Spano and Y. Olivier, *Phys. Rev. Lett.*, 2013, **110**, 226402.
52.H. Yamagata, C. M. Pochas and F. C. Spano, *J. Phys. Chem. B*, 2012, **116**, 14494-14503.